Intercore crosstalk in direct-detection homogeneous multicore fiber systems impaired by laser phase noise

TIAGO M. F. ALVES,[1,*] ADOLFO V. T. CARTAXO,[1,3] RUBEN S. LUÍS,[2] BENJAMIN J. PUTTNAM,[2] YOSHINARI AWAJI,[2] AND NAOYA WADA[2]

[1] *Instituto de Telecomunicações, 1049-001 Lisbon, Portugal*
[2] *Photonic Network System Laboratory, National Institute of Information and Communication Technology, Tokyo 184-8759, Japan*
[3] *ISCTE - Instituto Universitário de Lisboa, 1649-026 Lisbon, Portugal*
[*] *tiago.alves@lx.it.pt*

Abstract: The impact of the laser phase noise on the photodetected intercore crosstalk and performance of direct-detection orthogonal frequency division multiplexing multicore fiber systems is experimentally investigated. A new solution to overcome the performance fluctuations over time induced by the combined effect of laser phaser noise and intercore crosstalk is proposed. The solution uses adaptive modulation with extended time memory to estimate the bit loading scheme of each subcarrier from the mean and maximum error vector magnitude evaluated over the last ten blocks of transmitted training symbols. During measurements of up to 90 hours, intercore crosstalk power variation induced by fast laser phase noise variations exceeded 20 dB in both time and frequency, and error vector magnitude fluctuations of 4 dB were observed on a sub-second timescale. It is shown that direct-detection orthogonal frequency division multiplexing multicore fiber based systems employing a typical adaptive modulation solution, in which the bit loading scheme is evaluated from a single set of training symbols, suffer from unacceptable outage probabilities and are unable to counteract the fast power variations of intercore crosstalk and phase noise induced impairments. By extending the system memory used to estimate the bit loading scheme employed by the adaptive technique, an outage probability reduction by one order of magnitude is achieved. This reduction is attained by using the mean of the error vector magnitude evaluated over the last ten blocks of training symbols to estimate the bit loading scheme of subcarriers. Further reduction of the outage probability by four orders of magnitude is also demonstrated using a more conservative approach to estimate the bit loading scheme of the subcarriers. However, this conservative approach, based on the maximum error vector magnitude, may lead to additional loss of the average throughput.

References and links

1. Z. Feng, B. Li, M. Tang, L. Gan, R. Wang, R. Lin, Z. Xu, S. Fu, L. Deng, W. Tong, S. Long, L. Zhang, H. Zhou, R. Zhang, S. Liu, and P. Shum, "Multicore-fiber-enabled WSDM optical access network with centralized carrier delivery and RSOA-based adaptive modulation," Photon. J. **7**(4), 7201309 (2015).
2. M. Morant, A. Macho, and R. Llorente, "On the suitability of multicore fiber for LTE-advanced MIMO optical fronthaul systems," J. Lightwave Technol. **34**(2), 676–682 (2015).
3. J. Galvé, I. Gasulla, S. Sales, and J. Capmany, "Reconfigurable radio access networks using multicore fibers," J. Quantum Electr. **52**(1), 0600507 (2016).
4. H. Takahashi, K. Igarashi, and T. Tsuritani, "Long-haul transmission using multicore fibers," in Optical Fiber Communication Conference, OSA Technical Digest (Optical Society of America, 2014), paper Tu2J.2.
5. D. Butler, M. Li, S. Li, Y. Geng, R. Khrapko, R. Modavis, V. Nazarov, and A. Koklyushkin, "Space division multiplexing in short reach optical interconnects," J. Lightwave Technol. DOI 10.1109/JLT.2016.2619981 (2017).
6. B. J. Puttnam, R. Luís, E. Agrell, G. Rademacher, J. Sakaguchi, W. Klaus, G. Saridis, Y. Awaji, and N. Wada, "High capacity transmission systems using homogeneous multi-core fibers," J. Lightwave Technol. **35**(6), 1157–1167 (2017).
7. T. Kobayashi, M. Nakamura, F. Hamaoka, K. Shibahara, T. Mizuno, A. Sano, H. Kawakami, A. Isoda, M. Nagatani, H. Yamazaki, Y. Miyamoto, Y. Amma, Y. Sasaki, K. Takenaga, K. Aikawa, K. Saitoh, Y. Jung, D. Richardson, K.

Pulverer, M. Bohn, M. Nooruzzaman, and T. Morioka, "1-Pb/s (32 SDM/46 WDM/768 Gb/s) C-band dense SDM transmission over 205.6-km of single-mode heterogeneous multi-core fiber using 96-Gbaud PDM-16QAM channels," in Optical Fiber Communication Conference, OSA Technical Digest (Optical Society of America, 2017), paper Th5B.1.

8. D. Richardson, J. Fini, and L. Nelson, "Space-division multiplexing in optical fibres," Nat. Photon. **7**, 354–362 (2011).

9. R. Luís, B. J. Puttnam, A. Cartaxo, W. Klaus, J. Mendinueta, Y. Awaji, N. Wada, T. Nakanishi, T. Hayashi, and T. Sasaki, "Time and modulation frequency dependence of crosstalk in homogeneous multi-core fibers," J. Lightwave Technol. **34**(2), 441–447 (2016).

10. M. Koshiba, K. Saitoh, K. Takenaga, and S. Matsuo, "Analytical expression of average power-coupling coefficients for estimating intercore crosstalk in multicore fibers," Photon. J. **4**(5), 1987–1995 (2012).

11. T. Hayashi, T. Taru, O. Shimakawa, T. Sasaki, and E. Sasaoka, "Design and fabrication of ultra-low crosstalk and low-loss multi-core fiber," Optics Express **19**(17), 16576–16592 (2011).

12. A. Cartaxo, R. Luís, B. Puttnam, T. Hayashi, Y. Awaji, and N. Wada, "Dispersion impact on the crosstalk amplitude response of homogeneous multi-core fibers," Photon. Technol. Lett. **28**(17), 1858–1861 (2016).

13. A. Cartaxo and T. Alves, "Discrete changes model of inter-core crosstalk of real homogeneous multi-core fibers," J. Lightwave Technol. DOI 10.1109/JLT.2017.2652067 (2017).

14. T. Alves and A. Cartaxo, "Theoretical modelling of random time nature of inter-core crosstalk in multicore fibers," Proc. of IEEE Photonics Conference (IPC), paper WB2.4 (2016).

15. T. Alves and A. Cartaxo, "Inter-core crosstalk in homogeneous multi-core fibers: theoretical characterization of stochastic time evolution," J. Lightwave Technol. DOI 10.1109/JLT.2017.2754218 (2017).

16. G. Rademacher, B. J. Puttnam, R. Luís, Y. Awaji, and N. Wada, "Time-dependent inter-core crosstalk between multiple cores of a homogeneous multi-core fiber," Proc. of Asia Communications and Photonics Conference (ACPC), paper AF1D.2 (2016).

17. G. Rademacher, R. Luís, B. J. Puttnam, Y. Awaji, and N. Wada, "Crosstalk dynamics in multi-core fibers," Optics Express **25**(10), 12020–12028 (2017).

18. T. Alves, R. Luís, B. J. Puttnam, A. Cartaxo, Y. Awaji, and N. Wada, "Performance of adaptive DD-OFDM multicore fiber links and its relation with intercore crosstalk," Optics Express **25**(13), 16017–16027 (2017).

19. T. Alves, A. Cartaxo, R. Luís, B. J. Puttnam, Y. Awaji, and N. Wada, "Adaptive loading with extended memory to relax the impact of the phase noise-impaired ICXT in DD-OFDM MCF-based systems," Proc. of International Conference on Transparent Optical Networks (ICTON), paper Tu.D1.2 (2017).

20. A. Cartaxo, T. Alves, B. J. Puttnam, R. Luís, Y. Awaji, and N. Wada, "DD-OFDM multicore fiber systems impaired by intercore crosstalk and laser phase noise," Proc. of International Conference on Transparent Optical Networks (ICTON), paper Tu.D1.1 (2017).

21. B. J. Puttnam, R. Luís, T. Eriksson, W. Klaus, J. Mendinueta, Y. Awaji, and N. Wada, "Impact of intercore crosstalk on the transmission distance of QAM formats in multicore fibers," Photon. J. **8**(2), 0601109 (2016).

22. J. Pedro, R. Luís, B. J. Puttnam, Y. Awaji, N. Wada, and A. Cartaxo, "Experimental assessment of the time-varying impact of multi-core fiber crosstalk on a SSB-OFDM Signal," Proc. of Photonics in Switching (PS), 166–168 (2015).

23. J. He, B. Li, L. Deng, M. Tang, L. Gan, S. Fu, P. Shum, and D. Liu, "Experimental investigation of inter-core crosstalk of MIMO-OFDM/OQAM radio over multicore fiber system," Optics Express **24***12*, 13418–13428 (2016).

24. T. Alves and A. Cartaxo, "100-Gb/s DD-MB-OFDM metro network with 11-Gb/s granularity and 2.85-GHz receiver," Photon. Technol. Lett. **27**(24), 2551–2554 (2015).

25. R. Soeiro, T. Alves and A. Cartaxo, "Dual polarization discrete changes model of inter-core crosstalk in multi-core fibers," Photon. Technol. Lett. **29**(16), 1395–1398 (2017).

26. T. Hayashi, T. Taru, O. Shimakawa, T. Sasaki, and E. Sasaoka, "Characterization of crosstalk in ultra-low-crosstalk multi-core fiber," J. Lightwave Technol. **30**(4), 583–589 (2012).

27. J. Sakaguchi, B. J. Puttnam, W. Klaus, Y. Awaji, N. Wada, A. Kanno, T. Kawanishi, K. Imamura, H. Inaba, K. Mukasa, R. Sugizaki, T. Kobayashi, and M. Watanabe, "305 Tb/s space division multiplexed transmission using homogeneous 19-core fiber," J. Lightwave Technol. **31**(4), 554–562 (2013).

28. T. Imai and T. Matsumoto, "Polarization fluctuations in a single-mode optical fiber," J. Lightwave Technol. **6**(9), 1366–1375 (1988).

29. M. Karlsson, J. Brentel, and P. Andrekson, "Long-term measurement of PMD and polarization drift in installed fibers," J. Lightwave Technol. **18**(7), 941–951 (2000).

30. C. Tremblay, A. Michel, M. Tanoh, M. Bélanger, S. Clarke, D. Charlton, D. Peterson, and G. Wellbrock, "Dynamics of polarization fluctuations in aerial and buried links," Proc. of International Conference on Transparent Optical Networks (ICTON), paper We.B1.2 (2017).

31. P. Krummrich and K. Kotten, "Extremely fast (microsecond timescale) polarization changes in high speed long haul WDM transmission systems," in Optical Fiber Communication Conference, OSA Technical Digest (Optical Society of America, 2004), paper OWI40.

32. G. Soliman, M. Reimer, and D. Yevick, "Measurement and simulation of polarization transients in dispersion compensation modules," J. Opt. Soc. Am. A **27**(12), 2532–2541 (2010).

33. P. Krummrich, E. Schmidt, W. Weiershausen, and A. Mattheus, "Field trial results on statistics of fast polarization changes in long haul WDM transmission systems," in Optical Fiber Communication Conference, OSA Technical

Digest (Optical Society of America, 2005), paper OThT6.

34. S. Betti, G. De Marchis and E. Iannone, *Coherent Optical Communications Systems* (John Wiley & Sons, 1995), Chap. 4.

35. N. Cvijetic, S. Wilson, and D. Qian, "System outage probability due to PMD in high-speed optical OFDM transmission," J. Lightwave Technol. **26**(14), 2118–2127 (2008).

1. Introduction

Space-division multiplexing (SDM) systems based on multicore fibers (MCFs) have been recently proposed for access networks [1], radio-over-fiber [2, 3], long-haul networks [4] and intra data centers communications [5]. These systems may be developed using homogeneous MCFs, as they are simple to fabricate and can offer some system advantages such as use of spatial super channels, simplified digital signal processing or switching [6], or heterogeneous MCFs that are characterized by lower intercore crosstalk (ICXT) levels and also support large transmission throughput [7].

The ICXT due to mode coupling between cores is a potential limitation of some kinds of SDM systems employing MCFs [8]. Recently, the short term average crosstalk (STAXT) and the crosstalk transfer function (XTTF) were experimentally analyzed and discussed [9]. Large fluctuations of the STAXT along time and of the XTTF amplitude in both time and frequency were observed. In recent years, simple models to estimate theoretically the ICXT variation along the longitudinal direction of the MCF [10–13] and over time [14–16] have been reported. The longitudinal variation of the ICXT is attributed to perturbations of the MCF structure [11] and the random time nature of ICXT is attributed to change of these perturbations in time due to the modification of environmental conditions. Most of the ICXT characterizations performed so far used continuous wave (CW) or a single modulated tone as interfering crosstalk signal. Recently, the time-dependence of the ICXT in a homogeneous MCF has been theoretically and experimentally studied considering signals with various modulation formats and symbol rates [17–19]. It was concluded that MCF-based systems employing carrier free signals, such as quadrature amplitude modulation (QAM) typical of long-haul links, exhibit nearly constant ICXT power over time [17]. In contrast, direct detection (DD) MCF-based systems using carrier supported signals are impaired by ICXT power that may fluctuate significantly over time and require an additional performance margin to operate adequately [17, 18]. In DD-MCF-based systems using carrier supported modulation formats, the signal transmitted in a given core is recovered after the beating between the data and optical carrier signals transmitted in the same core (test core) according to the photodetector square law. Similarly, the ICXT affecting the photodetected signal results mainly from the beating between the ICXT generated by the interfering cores and the optical carrier of the test core [18, 20]. Assuming the use of distinct incoherent light sources for transmission of the signals of the test and interfering cores, the photodetected ICXT (P-ICXT) results from the beating between two signals with independent phase noises. As a consequence, the design of ICXT mitigation techniques required to relax outage constraints in MCF-based systems needs to account for the impact of the laser phase noise on the time evolution of the ICXT.

In [21], the potential for the time varying nature of the ICXT to place an additional performance penalty on the long term operation of long-haul single carrier MCF-based systems was discussed. Although the time varying ICXT has not been monitored, it was concluded that adequate management of the average and dynamic properties of ICXT is crucial for the design of such systems and that more detailed studies are required to fully quantify its impact on the system performance. In [22], it was shown that the random time varying nature of ICXT caused a 7 dB performance penalty in a DD-OFDM-MCF-based system employing fixed modulation. In [18], experimental results obtained over a 210-hour period showed that the time evolution of the error vector magnitude (EVM) of DD orthogonal frequency-division multiplexing (OFDM) systems

due to the time varying ICXT can be suitably estimated from the normalized power of the P-ICXT. It was also shown that performance fluctuations due to the ICXT may be minimized resorting to adaptive modulation techniques and, in particular, that the adaptive OFDM is a viable solution to guarantee link quality in MCF-based systems. Several other works, dedicated to investigate the transmission capabilities of MCFs and exploiting adaptive techniques to mitigate the ICXT, were also reported [1–4, 8, 23]. However, none of those works investigated how the time evolution of the ICXT and of the system performance are affected by the laser phase noise. In [20], a preliminary study of the impact of the laser phase noise on the P-ICXT and on the performance of DD-OFDM MCF-based systems was performed experimentally and by simulation using a single polarization time varying ICXT model. From the conclusions drawn, a new adaptive modulation technique, based on the mean EVM of each subcarrier evaluated over a set of blocks of training symbols, to gain insight and mitigate the degradation induced by the combined effect of the laser phase noise and ICXT has been proposed and validated experimentally [19].

In this work, the impact of the P-ICXT on the performance of DD-OFDM MCF-based systems is investigated experimentally and by simulation. The P-ICXT and system performance impaired by the laser phase noise are monitored experimentally over almost four consecutive days in both time and frequency. The simulation studies are performed by using a dual polarization time varying ICXT model. A new adaptive modulation technique, based on the maximum EVM of each subcarrier evaluated over a set of blocks of training symbols, is proposed and compared with that one presented in [19]. The two adaptive solutions using extended time memory to estimate the bit loading schemes employed in the OFDM subcarriers are further exploited to relax the outage probability caused by the combined effect of the time varying ICXT and laser phase noise impairments.

2. Fluctuation of photodetected ICXT

2.1. Theory

Let us consider two independent channels that are transmitted over two cores of a DD-MCF-based system. We consider that the operating wavelength of the two channels is the same and that the waveforms of these channels are incoherent due to the use of different laser sources or due to the differences between the propagation path of the two channels. Each channel consists of a modulation signal bearing information data and the optical carrier (OC) required to assist the detection. The ICXT generated in the test core due to the signal transmitted in the interfering core consists of two main components: (i) the ICXT component originating from the OC of the interfering core and (ii) the ICXT component originating from the data signal of the interfering core. If we take the u_x and u_y polarization directions as a reference, the Jones vector of the optical signal at the output of the test core, $e_o(t)$, can be expressed as:

$$e_o(t) = [A_{t,x}(t) + s_{t,x}(t) + A_{XT,x}(t) + s_{XT,x}(t)]u_x +$$
$$+ [A_{t,y}(t) + s_{t,y}(t) + A_{XT,y}(t) + s_{XT,y}(t)]u_y \qquad (1)$$

where $A_{t,(x,y)}(t)$ and $s_{t,(x,y)}(t)$ are the OC and data signal of test core, respectively, along the u_x and u_y directions. $A_{XT,(x,y)}(t)$ and $s_{XT,(x,y)}(t)$ are the ICXT components originating from the OC and data signal of the interfering core, respectively, along the u_x and u_y directions. Typically, in conventional DD-OFDM systems, the power of the OC is much higher than the power of the data signal ($|A_{t,(x,y)}(t)|^2 \gg |s_{t,(x,y)}(t)|^2$) [24]. Considering that the ICXT signal power is much lower than the power of the signal transmitted in the test core and that the OFDM signal is slightly shifted away from DC to avoid the beating between the OC of the test core and the ICXT

originating from the OC of the interfering core, the P-ICXT can be approximated by [18]:

$$i_{XT}(t) \approx 2R_\lambda \mathfrak{R}\left\{A_{t,x}(t)s^*_{XT,x}(t) + A_{XT,x}(t)s^*_{XT,x}(t) + A_{t,y}(t)s^*_{XT,y}(t) + A_{XT,y}(t)s^*_{XT,y}(t)\right\}$$

$$(2)$$

where z^* stands for the conjugate of z, R_λ is the PIN responsivity and $\mathfrak{R}\{x\}$ is the real part of x. The first and third terms of Eq. (2) result from the beating between the OC launched into the test core and the ICXT originating from the data signal of the interfering core (OC-SXT beating) along the u_x and u_y directions. The second and fourth terms result from the beating between the ICXT originating from the OC and data signal of the interfering core (OCXT-SXT beating) along the u_x and u_y directions, respectively. The OCXT-SXT beating provides a good approximation of the XTTF, defined in [9], if a sinusoidal signal is considered at the input of the interfering core. In systems with similar optical powers launched into each core, $|A_{t,(x,y)}(t)|$ is much higher than $|A_{XT,(x,y)}(t)|$ in most of the time and the second and fourth terms of Eq. (2) can be neglected. In this case, the P-ICXT is approximated by:

$$i_{XT}(t) = i_{XT,x}(t) + i_{XT,y}(t) \approx 2R_\lambda \mathfrak{R}\left\{A_{t,x}(t)s^*_{XT,x}(t) + A_{t,y}(t)s^*_{XT,y}(t)\right\}$$

$$(3)$$

where $i_{XT,(x,y)}$ represent the contributions of the OC-SXT beatings along the u_x and u_y directions to the P-ICXT. If we neglect the fiber loss and the impact of the group velocity dispersion on the P-ICXT, the contributions of the OC-SXT beat signals in each polarization direction can be rewritten to make explicit the phase noise processes $\Phi_i(t)$ and $\Phi_t(t)$ of the distinct incoherent light sources used for transmitting the signals of the test and interfering cores:

$$i_{XT,(x,y)}(t) \approx 2R_\lambda \mathfrak{R}\{|A_{t,(x,y)}|\exp[j\Phi_t(t)]\{s^*_{i,(x,y)}(t)\exp[-j\Phi_i(t)]\} * h^*_{XT,(x,y)}(t)\}$$

$$(4)$$

where we have considered the ICXT originating from the data signal of the interfering core in u_x and u_y directions given by

$$s_{XT,(x,y)}(t) = \{s_{i,(x,y)}(t)\exp[j\Phi_i(t)]\} * h_{XT,(x,y)}(t)$$

$$(5)$$

and the OC of the test core given by

$$A_{t,(x,y)}(t) = |A_{t,(x,y)}|\exp[j\Phi_t(t)]$$

$$(6)$$

with $|A_{t,(x,y)}|$ the amplitude of CW optical field of the test core in the u_x and u_y directions, $s_{i,(x,y)}(t)$ the data signal injected in the interfering core in the u_x and u_y directions, and $*$ the convolution operator. The ICXT field impulse response, $h_{XT,(x,y)}(t)$, describes the time varying random ICXT mechanism in the u_x and u_y directions [12, 14, 25].

Equation (4) shows that the time variation of detected ICXT is caused by two independent sources: (i) the ICXT mechanism, that varies due to perturbations of the MCF structure and change of environmental conditions, and (ii) the phase noise induced by the laser sources. It should be noted that the scale of the time variation of these two effects is quite different. The ICXT mechanism varies in the scale of seconds or minutes [9, 16, 18, 26] whereas, for lasers with typical linewidths within the range of tens of kHz or few MHz, the time variation of the ICXT induced by the laser phase noise occurs in a μs scale.

2.2. Time evolution of the photodetected ICXT power

In this subsection, the magnitude of the contribution of the OC-SXT and OCXT-SXT terms of Eq. (2) to the P-ICXT is assessed experimentally. This is accomplished by measuring and comparing, after photodetection, the time evolution of the signal power received in the test core,
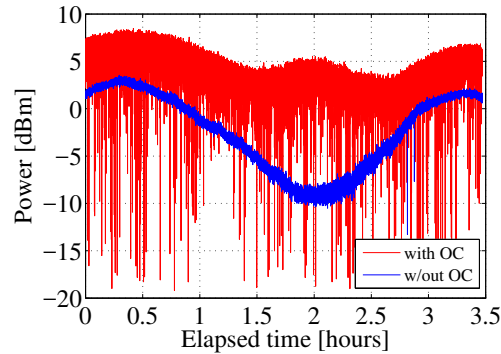
Fig. 1. Power of the received signal after photodetection of the test core signal with and without considering the transmission of the OC in the test core.

i. e., the P-ICXT power, in the following two conditions: (i) without launching signal into the test core, in which the P-ICXT is governed mainly by the OCXT-SXT beating, and (ii) launching the OC into the test core, which corresponds to a situation where the P-ICXT is given mainly by Eq. (2). The measurements corresponding to the two situations are taken sequentially with time intervals of 0.6 seconds. The modulation signal used in the interfering core is generated by a frequency synthesizer oscillating at 1 GHz. An external cavity laser (ECL) with linewidth of 100 kHz and a Mach-Zehnder modulator (MZM) biased 6 dB below the maximum power of its input-output characteristic are employed to generate the interfering and test signals. An optical amplifier at the MCF output is used to increase the power of the detected signal to measurable levels.

The MCF is a 10.1 km-long homogeneous trench-assisted 19-core fiber with cladding diameter of 200 μm, core pitch of 35 μm, coating diameter of 345 μm, average loss of 0.23 dB/km, normalized mean ICXT power of -32 dB [27] and a decorrelation time of the STAXT measured to be over 2 hours in lab conditions. With the short time interval between consecutive measurements we ensure that the time variation of the received power due to the ICXT mechanism is negligible between consecutive measurements. The optical power injected in the test and interfering cores is -3.5 dBm and 9 dBm, respectively. The higher power of the interfering core is required to obtain measurable detected ICXT power levels.

Figure 1 shows the time evolution of the received ICXT power after photodetection of the signal at the output of the test core with and without launching the OC into the test core. It is shown that the impact of the laser phase noise on the P-ICXT obtained by launching the OC into the test core is significantly different from that observed in the absence of OC. In the absence of OC, the P-ICXT is governed mainly by the XTTF and is characterized by power fluctuations whose timescale features are due to the ICXT mechanism. This is because the XTTF is originated from the beating between the ICXT originating from the OC and data signal of the interfering core which are both generated by the same laser and, thus, is weakly affected by the phase mismatch induced by the phase noise. The P-ICXT obtained when the OC is launched into the test core shows power fluctuations with two timescale variations. One, attributed to the ICXT mechanism, is observed in the time evolution of the ICXT power envelope and presents a slow time variation. The other, occurs randomly and with a much shorter time scale duration, and is attributed to the phase mismatch of the phase noises of the signals transmitted in the two cores and causes pronounced dips on the received ICXT power. These power dips correspond to ICXT power fluctuations that may exceed 20 dB. Although these observations have been made for systems employing lasers with linewidth of 100 kHz, faster fluctuations over time of the P-ICXT power are expected in systems employing lasers with larger linewidths. The analysis of Fig. 1
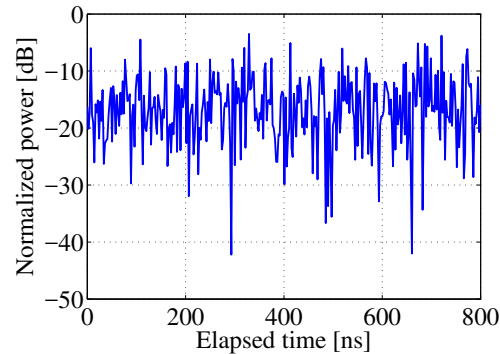
Fig. 2. Power of the P-ICXT measured over a short timescale interval.

also indicates that the OC-SXT beating term is dominant over the XTTF-dependent term in most of the 3.5 hour observation period. This result confirms that the P-ICXT in DD systems is predominantly due to the OC-SXT beating as considered in subsection 2.1.

The P-ICXT results shown in Fig. 1 were measured over a time period of a few hours with measurements taken at each 0.6 seconds. Additional measurements of the P-ICXT, taken in a microsecond period and with a sampling time between consecutive ICXT measurements of a few nanoseconds, have been also captured with the OC being transmitted in the test core. These measurements are depicted in Fig. 2 and show the fast fluctuations of the P-ICXT power which would be otherwise unnoticed. Significant P-ICXT power fluctuations occur in the short time period assessed with power dips of several dB being observed with time intervals of a few tens of nanoseconds. The duration of these time intervals is not compatible with the fluctuations induced by the ICXT mechanism, whose decorrelation time is of the order of several minutes, or with fluctuations caused by polarization changing. In sheltered environments, as ducts or lab facilities, polarization fluctuations are typically characterized by a timescale on the order of minutes or days [28–30]. Faster sub-milisecond polarization fluctuations are usually reported as isolated events caused by specific mechanical or atmospheric perturbations [30–33]. These perturbations were not observed during our lab experiments and the fluctuations of the room temperature did not exceed one degree Celsius.

2.3. *Spectrogram of photodetected ICXT*

In this subsection, the impact of the phase noise on the time and frequency evolution of the P-ICXT fluctuations is assessed by numerical simulation. Such as performed in section 2.2, the spectrograms of the normalized P-ICXT are evaluated in two situations. One, where the P-ICXT is evaluated from the OCXT-SXT beating and that enables obtaining, after adequate normalization, the XTTF. As performed in [9], this is obtained by launching an OC and a sinusoidal signal sweeping in frequency into the interfering core. Other, where the P-ICXT is evaluated by launching the OC also into the test core. In this case, the P-ICXT is dominated by the OC-SXT beating and, to differentiate from the XTTF, is defined, after normalization, as the carrier-crosstalk transfer function (CXTF). The CXTF is evaluated from the amplitude of the photodetected signal when an OC and a sinusoidal waveform are injected into the interfering core and the photodetection is assisted by the OC launched into the test core. The normalization factor of the spectrograms is the received average power in the absence of ICXT when a sinusoidal signal is launched in the test core. The simulation is performed considering the MCF used in [9] and the phase noise introduced by the continuous wave laser is modeled by a Wiener process [34] with zero mean and variance of $t\Delta v/(2\pi)$, where t represents the time and Δv=100 kHz is the
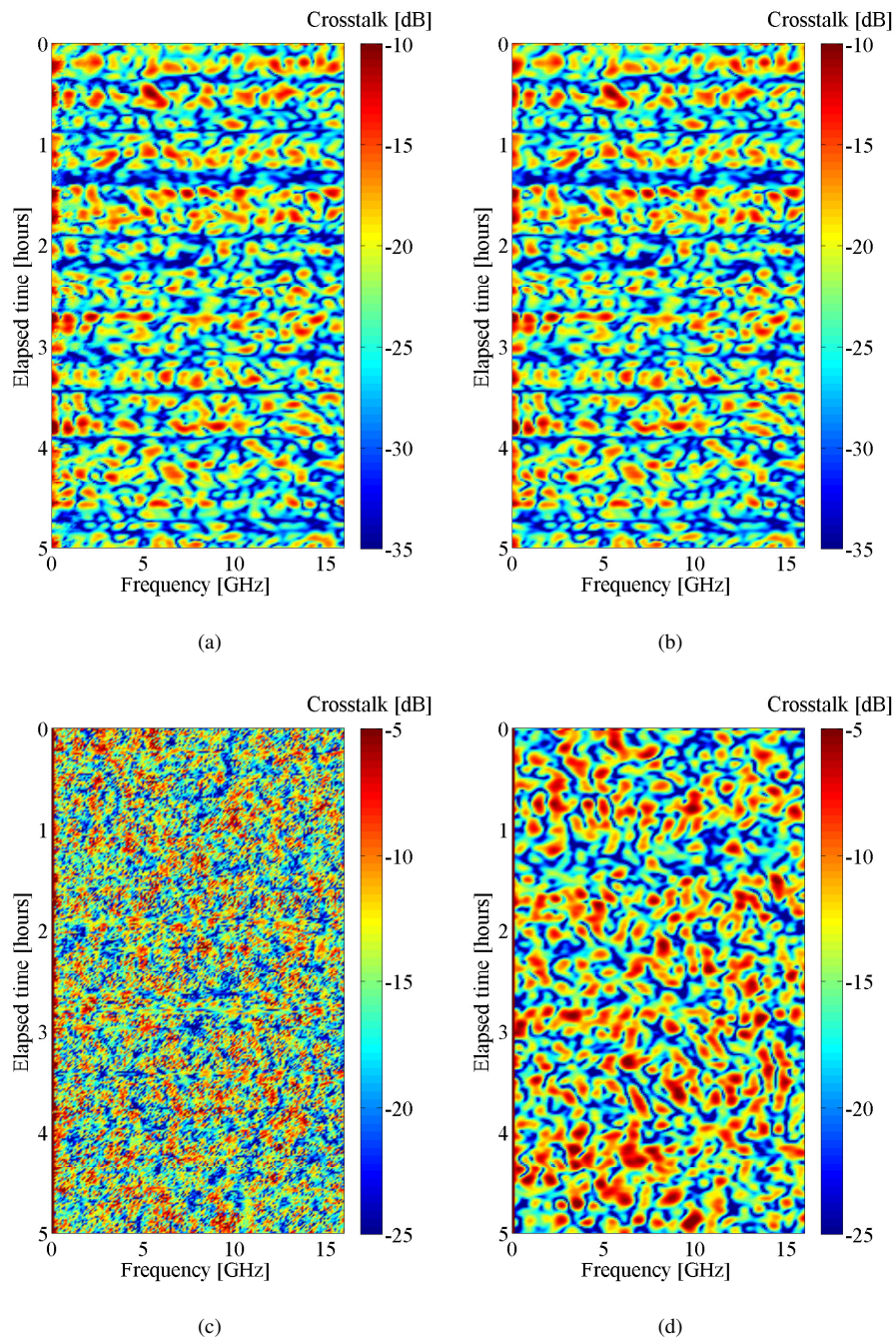
Fig. 3. Spectrograms of the normalized XTTF amplitude (a) with and (b) without considering the laser phase noise, and of the normalized CXTF amplitude (c) with and (d) without considering the laser phase noise.

laser linewidth. The time varying phase shift model of [14, 15] and the dual polarization ICXT model of [25] are considered in the simulation. The dual polarization ICXT model yields a more

accurate assessment of the impact of crosstalk on the system performance by taking the relative state of polarization of signal and crosstalk into account. The single-polarization case reported in [20] assumes co-polarized signal and crosstalk. The decorrelation time of each phase shift is set to 19 minutes, 1000 phase matching points (PMPs) are used, and the phase shift variance is 4π. Results for the pair of cores (5,4) characterized by a decorrelation time of 4.1 minutes and average skew of 1.579 ns are obtained. These parameters were chosen to match those of the MCF used in [9]. With this, a comparison between the simulation results obtained in this section and the spectrograms of the XTTF amplitude measured experimentally in [9] can be accomplished. Optical power with the same level is injected in the test and interfering cores. Figures 3(a) and 3(b) depict the spectrograms of the normalized XTTF amplitude with and without considering the laser phase noise effect, respectively. Figures 3(c) and 3(d) show the spectrograms of the normalized CXTF amplitude with and without considering the laser phase noise effect, respectively. The same Brownian motion for the time evolution of the phase shifts of each PMP is used in the four spectrograms. This is equivalent to obtain the ICXT power for each time/frequency pair of the four spectrograms sequentially in a short time interval over which the ICXT power remains unchanged. Hence, attention is paid only to the impact of the laser phase noise on the time evolution of the P-ICXT. Two main conclusions are drawn from the inspection of Fig. 3. (i) The spectrograms of the XTTF amplitude with and without considering the impact of the laser phase noise shown in Figs. 3(a) and 3(b) are very similar because the XTTF results from the beating between the ICXT originating from the OC and data signal generated by the same laser source, as explained in subsection 2.1. The spectrograms of the XTTF amplitude with and without considering the laser phase noise are not exactly the same due to slight differences of the normalized XTTF amplitude that occur at the lower frequencies [20]. These differences are small and are not easily observed in Fig. 3(a). At the lower frequencies, the period of the sinusoidal waveform used to obtain the spectrograms and the timescale of the variation of the laser phase noise are of the same magnitude and, therefore, some phase-to-intensity noise conversion induced by the ICXT field impulse response occurs. At the higher frequencies, the period of the sinusoidal waveform is much shorter than the timescale of the variation of the laser phase noise and the phase-to-intensity noise conversion due to the ICXT field impulse response is negligible. (ii) In DD MCF-based systems with the P-ICXT predominantly impaired by the OC-SXT contribution, CXTF power dips induced by the laser phase noise and exceeding 20 dB occur frequently along time and frequency, as shown in Fig. 3(c). These dips change the time and frequency behavior of the ICXT power fluctuations reported in [9] as they occur in time intervals and in frequency ranges much shorter than the ones that characterize the time and frequency variation induced by the ICXT mechanism itself. In the absence of the laser phase noise, the dips are not observed in the spectrogram of the normalized CXTF amplitude, as shown in Fig. 3(d). These results show that change of the time and frequency behavior of the ICXT power fluctuations caused by the laser phase noise can have a large impact in adaptive DD-MCF based systems. Hence, proper adaptive ICXT mitigation techniques, prepared to deal with such large and fast fluctuations, are required for successful implementation of such systems.

3. Experimental DD-OFDM MCF system impaired by ICXT and laser phase noise

The design of adaptive techniques to minimize the impact of the ICXT on the DD-OFDM MCF-based system performance must be accomplished considering the fast time and frequency variation of the P-ICXT power induced by the phase mismatch resulting from laser phase noise. Hence, it is not sufficient to resort to adaptive techniques operating on the seconds to minutes timescale typical of ICXT power variation. In this section, we propose and experimentally demonstrate a new adaptive technique for DD-OFDM MCF-based links with extended time memory to counteract the impact of the combined effect of time varying ICXT and laser phase noise on the system performance.

3.1. Setup
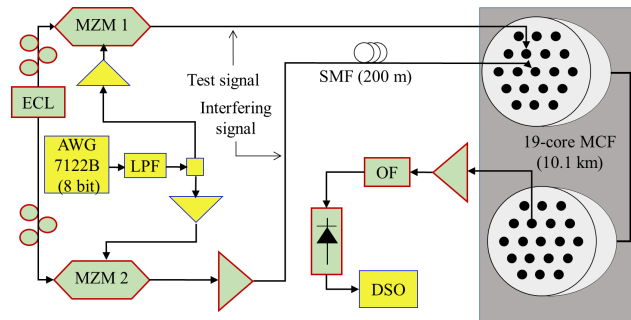
Fig. 4. Experimental setup used to measure the ICXT and the performance of adaptive DD-OFDM-based MCF systems in presence of laser phase noise. AWG: arbitrary waveform generator; DSO: digital storage oscilloscope; ECL: external cavity laser; LPF: low-pass filter; MCF: multicore fiber; MZM: Mach-Zehnder modulator; OF: optical filter; SMF: single-mode fiber.

Figure 4 shows the experimental setup deployed to measure the performance of the adaptive DD-OFDM MCF-based system. The analogue OFDM waveform was generated using an arbitrary waveform generator (AWG) operating at 20 Gsamples/s. The bandwidth of the OFDM signal was 2.5 GHz and the center frequency was 1.45 GHz. The OFDM signal consists of 1000 data symbols and 100 training symbols, each OFDM symbol consists of 128 subcarriers and different symbols were used in each of several separate time measurements. The QAM mappings available for each subcarrier were 4, 16, 32 or 64. Due to the unavailability of an additional AWG in the laboratory, we used the same OFDM signal in the test and interfering cores. The interfering and test optical signals were generated using the same ECL of section 2.2 with a maximum output power of 8 dBm, and single-arm MZMs biased 6 dB below the maximum power of their input-output characteristic to avoid significant signal-signal beat interference. After amplification, the power of the OC at the interfering core input was 9 dBm. The power of the OC injected in the test core was -3.5 dBm. A single-mode fiber with 200 m (corresponding to a time lag of 20 OFDM symbols) was used at the interfering core input to decorrelate the two OFDM signals. The characteristics of the 19-core MCF used in the experiments were introduced in section 2.2. An optical filter with a bandwidth of 0.15 nm was employed at the receiver side to reduce the out-of-band noise power and to prevent damaging the PIN photodetector. The OFDM signal was photodetected by a 16 GHz PIN and captured by a 12 GHz oscilloscope operating at 20 Gsamples/s. Offline processing was used for OFDM frame synchronization, cyclic prefix extraction, fast Fourier transform, one-tap frequency domain equalization and performance assessment.

The performance of the OFDM signal was measured over 90 hours. In each measurement, taken at 2.1 minute intervals, a OFDM signal with 1100 symbols carrying random data was transmitted and demodulated. The measured ICXT decorrelation time of the cores under analysis exceeds 2 hours. For this reason, in time intervals of 2.1 minutes, the ICXT is highly correlated and fluctuations of the system performance due to the ICXT mechanism between consecutive measurements are small.

3.2. Spectrograms of the CXTF corrupted by laser phase noise

This subsection shows experimentally obtained spectrograms of the normalized CXTF amplitude impaired by the laser phase noise. As shown in section 2.1, the P-ICXT is dominated by the OC-SXT beating term. Thus, only the OC is launched into the test core. To obtain the frequency dependence of the CXTF, a sinusoidal signal is launched into the interfering core. This signal is
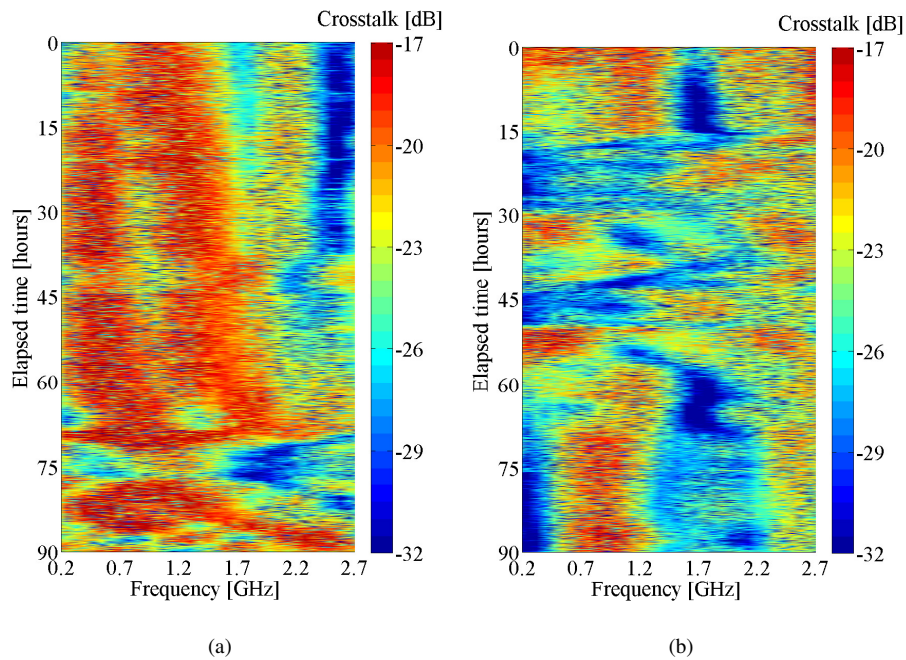
Fig. 5. Experimental spectrograms of the normalized CXTF amplitude measured over two 90 hour periods taken in two different weeks: (a) period A and (b) period B.

generated by using a frequency synthesizer in place of the AWG shown in Fig. 4. The frequency of the sinusoidal signal is sweeping along the bandwidth of the OFDM signal (between 200 MHz and 2.7 GHz). Signal power loading is employed in the generator to remove the limited frequency response of the electrical circuitry.

Figure 5 shows the experimental spectrograms of the normalized CXTF amplitude measured over two 90 hour periods taken in two different weeks: period A and period B. Variations of the normalized CXTF amplitude induced by the laser phase noise can be observed. As obtained by simulation in Fig. 3(c), these variations occur in time intervals and in frequency ranges much shorter than those typical of time and frequency variations induced by ICXT. It is also shown that the ICXT mechanism induces random power fluctuations on the P-ICXT along time and bandwidth of the OFDM signal of 15 dB. These conclusions are in agreement with the simulation analysis performed in section 2.3 and suggest that adaptive loading techniques are required to relax the performance degradation induced by the combined effect of ICXT and laser phase noise on the OFDM subcarriers.

3.3. Performance of adaptive modulation with extended memory

Three adaptive bit loading approaches to relax the time dependence and improve the performance of DD-OFDM systems impaired by ICXT and laser phase noise are assessed. The first is a reference approach, in which the bit loading of each OFDM subcarrier is estimated from the EVM of each subcarrier measured in the block of training symbols of the last measurement. In the second and third approaches, the bit loading of the OFDM subcarriers is estimated from the mean and maximum EVM of each subcarrier, respectively, evaluated over the blocks of training symbols from the last ten measurements. The ten measurements correspond to a time interval close to 20 minutes and comprise system performance measurements obtained under different

Start

An OFDM frame comprising 1000 data symbols and 100 training symbols is transmitted at every 2.1 minutes. In the first ten frames, 16-QAM mapping is used in all OFDM subcarriers.

Update the QAM mapping of each OFDM subcarrier.

At the receiver, each OFDM frame is demodulated and the EVM of each subcarrier is evaluated from the measured training symbols. The EVM of each subcarrier obtained in each measurement is recorded.

Identify, from the mean or maximum EVM and from the desired BER threshold, the more efficient QAM mapping allowed in each subcarrier.

How many frames were transmitted?

<10

≥10

Evaluate the mean or maximum EVM of each subcarrier from the EVMs recorded in the last ten measurements.

Fig. 6. Flowchart describing the adaptive bit loading approach with extended time memory.

levels of the time varying ICXT and phase noise random effects. Figure 6 shows a flowchart of the adaptive bit loading scheme employed in the second and third approaches. The scheme used in the first approach is similar to that of Fig. 6 but with the bit loading of each subcarrier estimated from the EVM of each subcarrier measured in the block of training symbols of the last measurement. Note that a feedback path between the receiver and the transmitter of the DD-OFDM system is required to inform the transmitter about the bit mapping that must be employed in each subcarrier. The period of the bit mapping updating should be shorter than the time scale of the ICXT variation. In this work, this information is transmitted once at each 2.1 minutes and, therefore, the feedback path requires a very low data-rate that may be transmitted in the management channel. With the extended time memory of the EVM employed in these two last approaches, we aim at mitigating the performance fluctuation caused by estimating the bit loading of the OFDM subcarriers at a given time instant and apply that bit loading to the OFDM subcarriers at a different time instant in which the P-ICXT may suffer from a large power variation due to the phase mismatch induced by the laser phase noise. The target bit error ratio (BER) for each adaptive approach is $3.8 \times 10^{-3} = 10^{-2.4}$. This BER level corresponds to the two interleaved extended BCH(1020,988) 7%-forward error correction (FEC) codes BER threshold (ITU-T G.975.1 rec.) and is evaluated from the mean of BER over all the OFDM subcarriers.

   Figure 7 depicts the EVM, BER and throughput of the OFDM signal when the bit loading of each subcarrier is obtained from the EVM evaluated using the last block of training symbols. Figure 7(a) clearly shows the impact of the combined effect of ICXT and phase mismatch induced by the laser phase noise on system performance. A time variation of the EVM induced by the ICXT mechanism of almost 5 dB is observed along the measurement period. In addition to this variation that occurs in a scale of tens of minutes, fast EVM fluctuations due to the laser phase noise are also observed. These fast EVM fluctuations can exceed 3 dB in consecutive measurements and originate from fast P-ICXT power variation induced by laser phase noise.

The bit loading estimated in instant t_1 may not be suitable at instant $t_2=t_1 + \Delta t$, with Δt the time interval between consecutive measurements, due to the ICXT power fluctuations. As a consequence, the performance of the adaptive OFDM signal transmitted in instant t_2 becomes degraded and the BER threshold of $10^{-2.4}$ is frequently surpassed, as shown in Fig. 7(b). The EVM evaluated from the training symbols transmitted in instant t_2 is then used to estimate the new bit loading scheme to be employed in instant $t_3=t_2 + \Delta t$. As the EVM in instant t_2 becomes degraded, less efficient QAM mappings are used in the new bit loading scheme to improve the system performance and, as a consequence, the throughput of instant t_3 decreases. This process occurs repeatedly over time and results in large throughput fluctuations shown in Fig. 7(c).
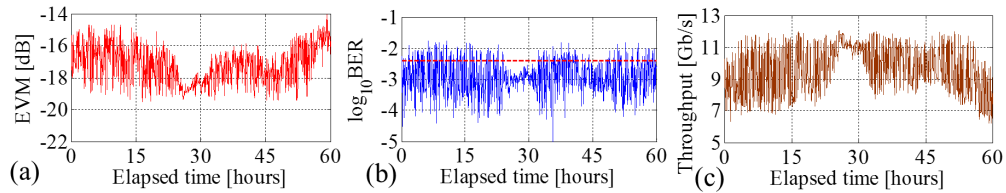
Fig. 7. (a) EVM, (b) BER and (c) throughput of the adaptive OFDM signal with the bit loading of each subcarrier obtained from the EVM of each subcarrier evaluated over the last block of training symbols.
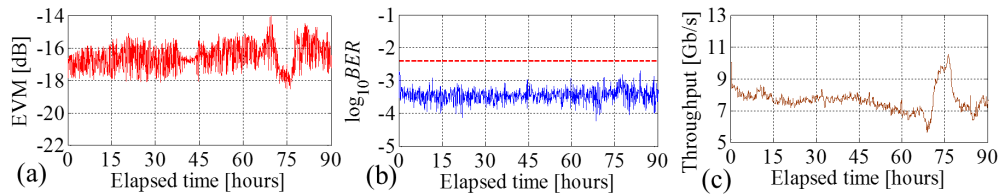
Fig. 8. (a) EVM, (b) BER and (c) throughput of the adaptive OFDM signal with the bit loading of each subcarrier obtained from the maximum EVM of each subcarrier evaluated over the last ten blocks of training symbols.
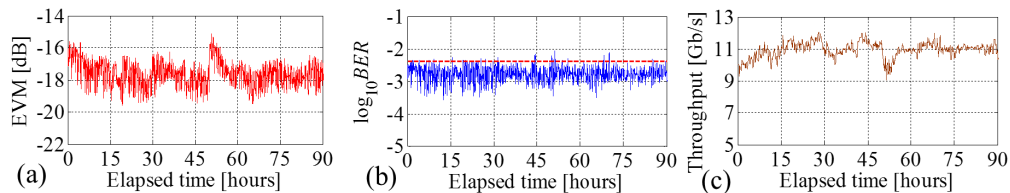
Fig. 9. (a) EVM, (b) BER and (c) throughput of the adaptive OFDM signal with the bit loading of each subcarrier obtained from the mean EVM of each subcarrier evaluated over the last ten blocks of training symbols.

Figures 8 and 9 show results similar to Fig. 7, but with the bit loading of each subcarrier estimated from the maximum and mean EVM of that subcarrier evaluated over the last ten measured blocks of training symbols, respectively. As a reference, the time and frequency variation of the normalized CXTF amplitude over the measurement period of Figs. 8 and 9 correspond to the normalized CXTF amplitude of period A and period B shown in Figs. 5(a) and

5(b), respectively. Figures 8 and 9 show that the two adaptive techniques with extended memory enable a significant decrease of the performance and throughput fluctuations over time. A BER that rarely surpasses the threshold in the 90 hour observation period is achieved with the adaptive technique in which the bit loading is estimated from the mean EVM calculated over the last ten blocks of training symbols. In fact, when the bit loading is estimated from the maximum EVM that occurs in the last ten blocks of training symbols, the BER never surpassed the threshold in the 90 hour period. However, this is obtained at the expense of a system throughput reduction.

Table 1. Throughput of the OFDM signal obtained when the adaptive techniques with extended memory are used.

Throughput [Gb/s]	Mean	Peak	Lowest
Bit Loading with "Mean EVM"	10.9	12.1	9.1
Bit Loading with "Maximum EVM"	7.7	10.8	5.6

Table 1 shows the throughput of the OFDM signal obtained when the adaptive techniques with extended memory are used. The adaptive DD-OFDM MCF link using the bit loading estimated from the mean EVM and maximum EVM shows a mean throughput of 10.9 Gb/s and 7.7 Gb/s, respectively. These mean throughputs represent a reduction of only 10% and 29% for the bit loading estimated from the mean EVM and maximum EVM, respectively, relative to the peak throughput. The relatively low average throughput achieved with the bit loading estimated from the maximum EVM of the last ten blocks of training symbols is not only due to the conservative estimation of the bit loading scheme provided by the maximum operator but also due to the higher power of the ICXT occurring over the 90 hour period, as suggested by Fig. 5(a). Without adaptive modulation, the lowest throughput achieved in the 90 hour period would be the required throughput that a static modulation scheme would need to be dimensioned for in order to operate without impairment in the measured time period. The results of Table 1 show an improvement of 20% and 38% for the bit loading estimated from the mean EVM and maximum EVM, respectively, relative to the throughput achieved by the static modulation system (lowest throughput in Table 1).
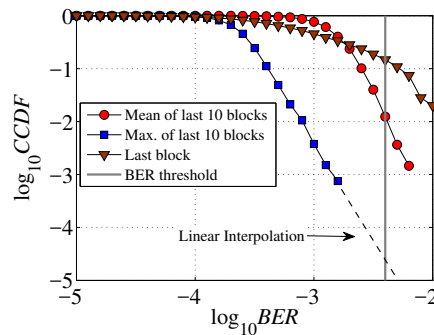
Fig. 10. CCDF of the BER obtained when the bit loading is estimated from the EVM evaluated in the last block of training symbols, and from the mean and maximum EVM evaluated over the last ten blocks of training symbols.

Figure 10 depicts the complementary cumulative density function (CCDF) of the BER obtained when the bit loading is estimated from the EVM evaluated in the last block of transmitted training symbols, and from the mean and maximum EVM evaluated over the last ten blocks of transmitted training symbols. Let us define the system outage probability when the CCDF evaluated from the mean BER across all the OFDM subcarriers [35] is equal to the 7%-FEC BER threshold. In

this situation, Fig. 10 shows that the proposed adaptive technique provides an outage probability improvement that exceeds one order of magnitude when the bit loading is estimated from the mean EVM and of almost four orders of magnitude when the bit loading is estimated from the maximum EVM. These results suggest that the performance fluctuation along time induced by the ICXT and the phase mismatch caused by the laser phase noise can be drastically reduced by using adaptive techniques with extended time memory.

4. Conclusion

The impact of the combined effect of the time varying ICXT and laser phase noise impairments on the performance of DD-OFDM MCF-based systems has been experimentally investigated. A new adaptive modulation solution with extended time memory has been proposed to mitigate the performance degradation induced by this combined effect.

Photodetected ICXT power variations induced by phase noise that exceed 20 dB have been observed over the observation period and with a time duration scale that is much shorter than the scale of the time variation typical of ICXT mechanism. These power dips cause large fluctuations of the system performance along time and lead to potentially unacceptable outage probabilities. Although these observations have been made for systems employing lasers with linewidth of 100 kHz, faster fluctuations over time of the photodetected ICXT and system performance are expected in systems employing lasers with larger linewidths. It has been shown that the performance fluctuation along time induced by the phase mismatch caused by the laser phase noise can be suitably overcome by extending the system memory used to estimate the bit loading scheme employed by the adaptive technique. Particularly, an improvement of the outage probability that exceeds one order of magnitude using the mean of the EVM evaluated over the last ten blocks of transmitted training symbols to estimate the bit loading scheme of OFDM subcarriers has been shown. Further tolerance to fluctuations of the system performance along time has been also achieved by using a more conservative adaptive modulation approach based on estimating the bit loading scheme from the maximum EVM of the last ten blocks of transmitted training symbols. With this approach, a reduction of four orders of magnitude on the outage probability has been attained at the expense of additional loss of the mean throughput. These results provide useful guidelines for the design of MCF systems using direct-detection OFDM formats.

Funding